VOLUME 102 | SUPPLEMENT 1 | MARCH 2022

LI

LABORATORY INVESTIGATION

THE BASIC AND TRANSLATIONAL PATHOLOGY RESEARCH JOURNAL

ABSTRACTS (1076–1088)

MEDICAL RENAL PATHOLOGY

2022

USCAP 111TH ANNUAL MEETING

REAL INTELLIGENCE

MARCH 19–24, 2022 LOS ANGELES, CALIFORNIA

Published by
SPRINGER NATURE
www.ModernPathology.org

USCAP
Creating a Better Pathologist
AN OFFICIAL JOURNAL OF THE UNITED STATES AND CANADIAN ACADEMY OF PATHOLOGY

EDUCATION COMMITTEE

Rhonda K. Yantiss
Chair

Kristin C. Jensen
Chair, CME Subcommittee

Laura C. Collins
Chair, Interactive Microscopy Subcommittee

Yuri Fedoriw
Short Course Coordinator

Ilan Weinreb
Chair, Subcommittee for Unique Live Course Offerings

Carla L. Ellis
Chair, DEI Subcommittee

Adebowale J. Adeniran
Kimberly H. Allison
Sarah M. Dry
William C. Faquin
Karen J. Fritchie
Jennifer B. Gordetsky
Levon Katsakhyan, Pathologist-in-Training
Melinda J. Lerwill
M. Beatriz S. Lopes
Julia R. Naso, Pathologist-in-Training
Liron Pantanowitz
Carlos Parra-Herran
Rajiv M. Patel
Charles "Matt" Quick
David F. Schaeffer
Lynette M. Sholl
Olga K. Weinberg
Maria Westerhoff

ABSTRACT REVIEW BOARD

Benjamin Adam
Oyedele Adeyi
Mariam Priya Alexander
Daniela Allende
Catalina Amador
Vijayalakshmi Ananthanarayanan
Tatjana Antic
Manju Aron
Roberto Barrios
Gregory R. Bean
Govind Bhagat
Luis Zabala Blanco
Michael Bonert
Alain C. Borczuk
Tamar C. Brandler
Eric Jason Burks
Kelly J. Butnor
Sarah M. Calkins
Weibiao Cao
Wenqing (Wendy) Cao
Barbara Ann Centeno
Joanna SY Chan
Kung-Chao Chang
Hao Chen
Wei Chen
Yunn-Yi Chen
Sarah Chiang
Soo-Jin Cho
Shefali Chopra
Nicole A. Cipriani
Cecilia Clement
Claudiu Cotta
Jennifer A. Cotter
Sonika M. Dahiya
Elizabeth G. Demicco
Katie Dennis
Jasreman Dhillon
Anand S. Dighe
Bojana Djordjevic
Michelle R. Downes
Charles G. Eberhart
Andrew G. Evans
Fang Fan
Julie C. Fanburg-Smith
Gelareh Farshid
Michael Feely
Susan A. Fineberg
Dennis J. Firchau
Gregory A. Fishbein
Agnes B. Fogo
Andrew L. Folpe
Danielle Fortuna
Billie Fyfe-Kirschner
Zeina Ghorab
Giovanna A. Giannico
Anthony J. Gill
Tamar A. Giorgadze
Alessio Giubellino
Carolyn Glass
Carmen R. Gomez-Fernandez
Shunyou Gong
Purva Gopal
Abha Goyal
Christopher C. Griffith
Ian S. Hagemann
Gillian Leigh Hale
Suntrea TG Hammer
Malini Harigopal
Kammi J. Henriksen
Jonas J. Heymann
Carlo Vincent Hojilla
Aaron R. Huber
Jabed Iqbal
Shilpa Jain
Vickie Y. Jo
Ivy John
Dan Jones
Ridas Juskevicius
Meghan E. Kapp
Nora Katabi
Francesca Khani
Joseph D. Khoury
Benjamin Kipp
Veronica E. Klepeis
Christian A. Kunder
Stefano La Rosa
Stephen M. Lagana
Keith K. Lai
Goo Lee
Michael Lee
Vasiliki Leventaki
Madelyn Lew
Faqian Li
Ying Li
Chieh-Yu Lin
Mikhail Lisovsky
Lesley C. Lomo
Fang-I Lu
aDeqin Ma
Varsha Manucha
Rachel Angelica Mariani
Brock Aaron Martin
David S. McClintock
Anne M. Mills
Richard N. Mitchell
Hiroshi Miyamoto
Kristen E. Muller
Priya Nagarajan
Navneet Narula
Michiya Nishino
Maura O'Neil
Scott Roland Owens
Burcin Pehlivanoglu
Deniz Peker Barclift
Avani Anil Pendse
Andre Pinto
Susan Prendeville
Carlos N. Prieto Granada
Peter Pytel
Stephen S. Raab
Emilian V. Racila
Stanley J. Radio
Santiago Ramon Y Cajal
Kaaren K Reichard
Jordan P. Reynolds
Lisa M. Rooper
Andrew Eric Rosenberg
Ozlen Saglam
Ankur R. Sangoi
Kurt B. Schaberg
Qiuying (Judy) Shi
Wonwoo Shon
Pratibha S. Shukla
Gabriel Sica
Alexa Siddon
Anthony Sisk
Kalliopi P. Siziopikou
Stephanie Lynn Skala
Maxwell L. Smith
Isaac H. Solomon
Wei Song
Simona Stolnicu
Adrian Suarez
Paul E. Swanson
Benjamin Jack Swanson
Sara Szabo
Gary H. Tozbikian
Gulisa Turashvili
Andrew T. Turk
Efsevia Vakiani
Paul VanderLaan
Hanlin L. Wang
Stephen C. Ward
Kevin M. Waters
Jaclyn C. Watkins
Shi Wei
Hannah Y. Wen
Kwun Wah Wen
Kristy Wolniak
Deyin Xing
Ya Xu
Shaofeng N. Yan
Zhaohai Yang
Yunshin Albert Yeh
Huina Zhang
Xuchen Zhang
Bihong Zhao
Lei Zhao

To cite abstracts in this publication, please use the following format: **Author A, Author B, Author C, et al. Abstract title (abs#). In "File Title."** ***Laboratory Investigation*** **2022; 102 (suppl 1): page#**

1076 Myeloperoxidase (MPO) Immunostaining Can Identify Endothelial Injury of Peritubular Capillaries and Glomeruli in Renal Antibody Mediated Rejection

Olabisi Afolayan-Oloye[1], Megan Moore[2], Wei Li[3], Hassan Kanaan[3], Ping Zhang[4]
[1]Beaumont Health System, Royal Oak, MI, [2]Oakland University William Beaumont School of Medicine, Rochester, MI, [3]Beaumont Health, Royal Oak, MI, [4]William Beaumont Hospital, Birmingham, MI

Disclosures: Olabisi Afolayan-Oloye: None; Megan Moore: None; Wei Li: None; Hassan Kanaan: None; Ping Zhang: None

Background: C4d positive staining in peritubular capillaries (PTC) of renal grafts has been used as a marker to support antibody mediated rejection (AMR), if there are morphologic changes of AMR and the renal recipient has positive donor specific antibody. But it is not clear if the C4d staining is related to any peritubular and glomerular injury during AMR. As injured endothelial cells can uptake the MPO into the endothelial cells, we used MPO immunostaining to highlight glomerular endothelial injury in crescentic glomerulonephritis previously. The goal of this study was to determine if there was an endothelial injury of PTC and glomeruli that can correlate with patients' elevated serum creatinine levels (sCr).

Design: The study included one group of negative native renal controls from tumor related nephrectomies (n=12), one group of transplant biopsies with borderline changes (BC) as transplant controls (n=19), and one group of renal transplant biopsies with AMR as the study group (acute/chronic, n=23). All three groups of cases were stained for MPO immunohistochemically and the MPO expressions in the endothelium of PTC and glomeruli were evaluated for staining intensity and % of involved capillaries; multiplying the intensity and the positive % generated the final combined scores (H score). These MPO indices were correlated with sCr.

Results: AMR group (3.72±0.45 mg/dl) had significantly higher sCr than native controls (0.89±0.06 mg/dl) and transplant controls (2.23±0.20 mg/dl). The native control group and the transplant controls showed no MPO expression in endothelium of glomeruli and PTC. However, there were MPO positive stains in the endothelial cells of both glomeruli (16/23 cases, 69.5%) and peritubular capillaries (17/23 cases, 73.9%) in the biopsies with AMR (Figure and Table). There were significant correlations between the peritubular MPO staining versus sCr (r=0.355 and p= 0.0106), and glomerular MPO staining versus sCr (r=0.355 and p=0.0106) (n=54 cases from three groups). Also the H scores of glomerular MPO expression were significantly correlated with that of peritubular MPO staining (r=0.645, and p=0.0001).

Cases of AMR	Age/Gender	Diagnosis	sCr (mg/dl)	G-MPO intensity, +G/total G	PTC-MPO intensity, %
1	39F	aAMR	0.90	2+, 7/14	2, 5%
2	69M	aAMR	5.43	0, 0/5	0, 0%
3	33F	aAMR	2.41	0, 0/8	0, 0%
4	51F	aAMR	6.02	1, 6/7	1, 5%
5	40M	aAMR	3.01	1+, 5/14	1, 5%
6	47M	aAMR	7.21	1, 14/18	1, 60%
7	61F	aAMR	1.98	1, 5/7	0, 0%
8	39M	aAMR	10.10	0, 0/5	0, 0%
9	48F	aAMR	4.90	0, 0/1	2, 10%
10	45M	aAMR	3.08	1+, 8/22	1, 10%
11	57M	cAMR	2.70	0, 0/7	0, 0%
12	45M	cAMR	2.05	1, 1/8	0, 0%
13	45M	cAMR	3.80	1, 2/3	1, 10%
14	36M	cAMR	6.93	2, 3/4	1, 50%
15	30M	cAMR	2.90	1, 1/2	2, 60%
16	56M	cAMR	1.50	1, 1/12	1, 20%
17	45F	cAMR	1.33	1, 3/6	2, 20%
18	63F	cAMR	1.60	1, 3/4	2, 40%
19	54M	cAMR	2.53	0, 0/5	1, 10%
20	46M	cAMR	3.80	0, 0/1	1, 5%
21	57M	cAMR	3.10	No G	2, 50%
22	43M	cAMR	7.32	1, 4/7	2, 40%
23	46F	cAMR	1.83	1, 2/6	1, 40%

Figure 1 - 1076

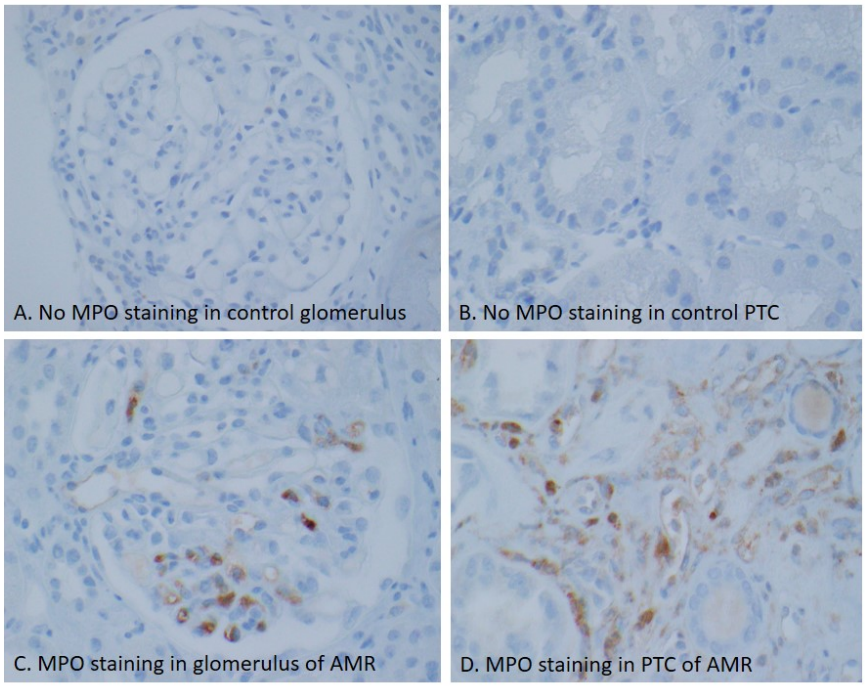

Conclusions: Our data indicate that MPO staining identified endothelial injuries in both glomeruli and PTC of AMR cases, which were significantly correlated with sCr. The endothelial injuries in both capillary beds may be related to C4d and other activated complement mediated damage during the AMR.

1077 Glomerular Segmentation and Classification Pipeline Using NEPTUNE Whole Slide Images

Akhil Ambekar[1], Bangchen Wang[2], Clarissa Cassol[3], Jarcy Zee[4], Xiang Li[1], Yijiang Chen[5], Ananya Rangavajla[6], Brinda Kapur[5], Lawrence Holzman[7], Jeffrey Hodgin[8], Laura Mariani[9], Anant Madabhushi[5], Kyle Lafata[1], Laura Barisoni[1], Andrew Janowczyk[5]

[1]Duke University, Durham, NC, [2]Duke University Medical Center, Durham, NC, [3]Arkana Laboratories, Little Rock, AR, [4]The Children's Hospital of Philadelphia, Perelman School of Medicine at the University of Pennsylvania, Philadelphia, PA, [5]Case Western Reserve University, Cleveland, OH, [6]CCIPD, Case Western Reserve University, Cleveland, OH, [7]Hospital of the University of Pennsylvania, Philadelphia, PA, [8]University of Michigan, Ann Arbor, MI, [9]Michigan Medicine, University of Michigan, Ann Arbor, MI

Disclosures: Akhil Ambekar: None; Bangchen Wang: None; Clarissa Cassol: None; Jarcy Zee: None; Xiang Li: None; Yijiang Chen: None; Ananya Rangavajla: None; Brinda Kapur: None; Lawrence Holzman: None; Jeffrey Hodgin: None; Laura Mariani: None; Anant Madabhushi: *Stock Ownership*, Inspirata Inc, Elucid Bioimaging; Kyle Lafata: None; Laura Barisoni: None; Andrew Janowczyk: None

Background: Detection and quantification of segmental and global glomerulosclerosis (SS and GS, respectively) in kidney biopsies has diagnostic and prognostic relevance. However, the use of conventional microscopy is time consuming, and carries limited accuracy and reproducibility of observations. To alleviate this problem, we developed a pipeline to automate the classification and quantification of SS, GS and non-GS/SS glomeruli.

Design: One Periodic acid Schiff whole slide image (WSI) from each of 188 kidney biopsies (53 minimal change disease, 97 focal segmental glomerulosclerosis, 24 membranous nephropathy, and 14 IgA nephropathy) from the NEPTUNE digital pathology repository were used. WSIs were divided into training (n=145) and testing (n=43) datasets and glomeruli were manually segmented by a pathology resident and a junior pathologist. Quality control of the segmentations was performed by a senior pathologist prior to their usage. Glomerular segmentations for SS, GS and non-GS/SS combined were used to train a deep learning (DL) model consisting of a 9-layer convolutional neural network based on U-Net architecture. An evaluation metric, Intersection Over Union

(IoU), was used to quantify the overlap between the manual and the predicted segmentations. A 5-layer DenseNet model was then trained to classify glomeruli into SS, GS and non-GS/SS. Model performance was measured using precision, recall and F1-score.

Results: Examples of manual and DL segmentations and classification outputs are shown in Figure 1. The mean IoU for the segmentation model in the training and testing set was 93.3% and 85% respectively. The classification model yielded an average precision, recall and F1-score of 93%, 95.3% and 93.6% in the training set and 86.1%, 83.9% and 84.7% in the testing set (for in-depth classification results see Figure 2). SS, GS, and non-GS/SS glomerular count is shown in Table 1.

	Manual Glom Count	U-Net Glom Count	Proportion Detected by U-Net
SS	72	60	83.3%
GS	120	87	72.5%
Non-GS/SS	674	587	87%
All Gloms	**866**	**734**	**84.7%**

Table 1: Glomerulus counts – Manual vs Automated: The proportion of SS and non-GS/SS glomeruli detected were >80%, whereas 72.5% of the GS glomeruli were detected. These results generated from the testing set show the promising nature of a DL system to detect all glomerulus types.

Figure 1 - 1077

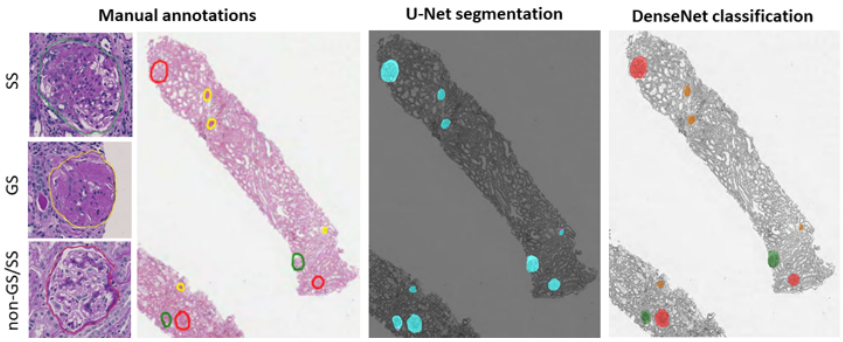

Figure 1: Glomerular segmentation and classification pipeline: Manual segmentation and classification, U-Net segmentation, and DenseNet classification pipeline for SS (green), GS (yellow) and non-GS/SS (red) glomeruli

Figure 2 - 1077

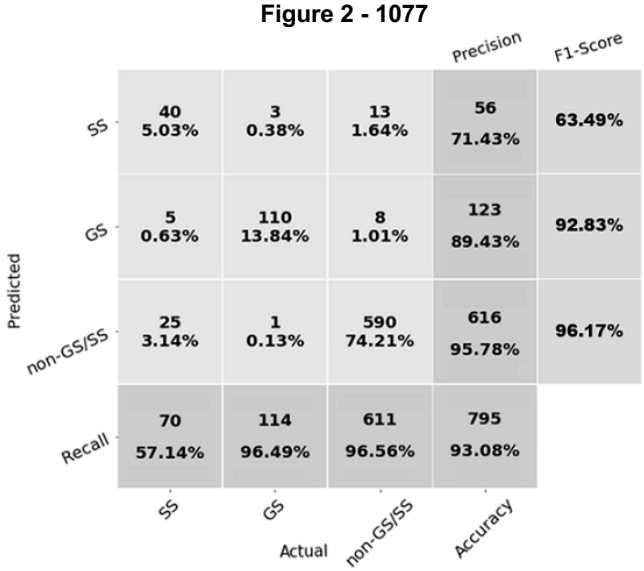

Figure 2: Confusion Matrix from DenseNet model in testing set: performance for the GS glomeruli and non-GS/SS glomeruli were around 90% by all measures, indicating robust performance. The performance for SS glomeruli was comparitively less robust with measures at around 60%

Conclusions: Our pipeline demonstrates a feasible and robust approach for automatic classification and quantification of SS, GS and non-GS/SS glomeruli.

1078 The Antigenic Landscape of Malignancy-Associated Membranous Nephropathy

Tiffany Caza[1], Samar Hassen[1], Chris Larsen[1]
[1]Arkana Laboratories, Little Rock, AR

Disclosures: Tiffany Caza: None; Samar Hassen: None; Chris Larsen: None

Background: Malignancy is a common secondary etiology of membranous nephropathy (MN). Patients with MN induced by an underlying tumor have poorer clinical outcomes and may not respond to immunosuppressive therapy. Recently, multiple new autoantigens were described in MN, which have not been comprehensively studied in the setting of malignancy-associated membranous nephropathy (M-A-MN). Here, we performed the largest study to date evaluating antigen types and histopathologic features of M-A-MN.

Design: A retrospective search of our case archives for kidney biopsies showing MN from patients with a history of cancer from 2015 to 2021 was performed. Kidney biopsies were immunostained for MN antigens, including phospholipase A2 receptor (PLA2R), thrombospondin type 1 domain containing 7a (THSD7A), neural epidermal growth factor-like 1 (NELL1), exostosin 1 (EXT1), serine protease HTRA1 (HTRA1), semaphorin 3B (SEMA3B), and neural cell adhesion molecule 1 (NCAM1). Clinical notes were evaluated to determine whether proteinuria correlates with underlying malignancy (recent or concurrent diagnosis, on chemo- or radiation therapy, or metastatic disease).

Results: A total of 5851 patients were diagnosed with MN from 2005-2021, of which 200 had a history of cancer (3.4%). Of the 200 cases, 155 had proteinuria correlate with an underlying malignancy (77.5%) and 45 patients had a remote cancer history or were in remission where MN was unlikely malignancy-associated (22.5%). The mean age of patients with M-A-MN was 67.9 ± 9.5 years and there was a male predominance (60.6%). Twenty-two patients (14.2%) had two primary cancers.

Of patients with M-A-MN, 22.5% were PLA2R+, 20.6% NELL1+, 6.4% THSD7A+, 1.3% EXT+, 0.6% HTRA1+, 0.6+ SEMA3B+, 0% NCAM1+, and 47.7% were of unknown antigen type. In the patients with MN with a history of malignancy without a temporal relationship, 76% were PLA2R+, 8.8% NELL1+, 2.2% EXT+, and 13.3% were of unknown antigen type, a similar distribution seen in 'primary' MN.

In M-A-MN cases of unknown antigen type, 18.9% demonstrated staining for IgA in subepithelial deposits, 29.7% IgM, 86.4% C3, 9.5% C1q, and 2.7% had 'full house' staining. Mesangial immune deposits were identified in 50.7% of cases and 7.5% of cases showed subendothelial deposits.

Conclusions: There remains a knowledge gap in the antigenic drivers of M-A-MN, with nearly half of cases being of unknown antigen type.

1079 Clinical Conundrum: Kidney Transplant Biopsies with Vasculitis in the Presence or Absence of SV40 Immunohistochemical Staining: A Descriptive Study

Ritu Gupta[1], Alton B. (Brad) Farris[2]
[1]Emory University Hospital, Atlanta, GA, [2]Emory University, Atlanta, GA

Disclosures: Ritu Gupta: None; Alton B. (Brad) Farris: None

Background: For-cause kidney transplant biopsies can show a vast array of findings at various time-points post-transplantation, with findings suggestive of humoral or cellular rejection as well as polyomavirus nephropathy due to BK viremia amongst the biggest clinical concerns. There is limited data regarding the simultaneous clinicopathologic diagnoses of polyomavirus nephropathy and humoral and/or cellular rejection in kidney transplant biopsies and the significant clinical conundrum they pose to the management of these patients.

Design: From 2015-2021, we identified 85 for-cause kidney transplant biopsies that showed vasculitis (v1 or v2 according to the Banff criteria) in combination with immunohistochemical SV40 testing in searching our institutional database. Of 8 cases with

vasculitis and positive SV40 immunohistochemical staining, 5 (62.5%) had recent negative HLA DSA testing and 3 (37.5%) had recent positive HLA DSA testing. The majority of the 8 biopsies were within 100-300 days post-transplantation. Of the 77 cases with vasculitis and negative SV40 immunohistochemical staining, 58 (75%) had recent negative HLA DSA testing and 19 (25%) had recent positive HLA DSA testing. For time-matched comparison (100-300 days post-transplantation), 6 total biopsies remained: 4 (66.7%) with negative HLA DSA testing and 2 (33.3%) with recent positive HLA DSA testing.

Results: By various analyses, no statistically significant data was obtained by comparison of the 2 cohorts (with or without SV40 immunohistochemical reactivity). A description of the cases is presented in Table 1.

Kidney Transplant Biopsies +/- SV40 IHC staining, Time to Biopsy, +/- HLA DSA, and Banff scores

Case	SV40	HLA DSA	Transplant-to-Biopsy (days)	v	t	i	g	ptc	C4d	ct	ci	cg	mm	cv	ah	ti	i-IFTA
1	Pos	No	287	1	3	2	0	0	0	0	0	0	0	0	0	N/A	N/A
2	Pos	No	161	1	3	3	1	0	0	3	3	0	1	1	1	N/A	N/A
3	Pos	No	160	1	3	3	2	3	0	1	2	1b	2	2	1	3	3
4	Pos	No	240	2	1	2	0	0	0	1	1	0	0	1	0	N/A	N/A
5	Pos	No	187	2	2	2	1	2	0	2	0	0	0	1	0	2	0
6	Pos	Yes	137	1	2	3	2	3	1	1	2	2	1	0	0	1	3
7	Pos	Yes	151	1	2	1	0	0	1	1	2	0	1	0	0	2	0
8	Pos	Yes	2354	1	2	3	2	3	1	3	1	0	2	0	1	3	2
9	Neg	No	123	1	3	2	1	3	0	1	1	0	0	1	1	2	3
10	Neg	No	254	1	2	2	2	1	0	1	1	0	3	0	2	2	2
11	Neg	No	119	2	3	3	2	0	0	0	0	0	0	0	0	N/A	N/A
12	Neg	No	101	2	3	3	0	0	0	0	0	0	2	0	0	N/A	N/A
13	Neg	Yes	182	1	3	3	2	1	2	1	2	0	0	0	0	3	3
14	Neg	Yes	198	1	3	1	2	2	1	1	0	0	0	1	0	1	0

Conclusions: For-cause kidney transplant biopsies with clinically opposing clinicopathologic diagnoses are rare and present a significant challenge to pathologists and clinicians alike in diagnosis and management of patients. This is the first known descriptive study presenting 2 cohorts with vasculitis (with or without SV40 immunohistochemical reactivity, each with or without HLA donor-specific antibodies). While differences between groups were not statistically significant, the small number of cases in each cohort may account for the lack of statistical differences; and furthermore, these findings point toward the fact that rejection and infection may be acting synergistically to contribute to allograft injury. Our study brings light to these challenging cases, highlights the need for physicians to be cognizant of the simultaneous findings, and supports the need for further research in this area of transplantation.

1080 An Epidemic of Serum Amyloid A Protein Amyloidosis Fueled by Injection Heroin Use - Associated Infections in the Pacific Northwest

David Henriquez Ticas[1], Shreeram Akilesh[1], Charles Alpers, MD[2], Behzad Najafian[1], Roberto Nicosia[1], Kelly Smith[1]
[1]University of Washington, Seattle, WA, [2]University of Washington School of Medicine, Seattle, WA

Disclosures: David Henriquez Ticas: None; Shreeram Akilesh: None; Charles Alpers, MD: None; Behzad Najafian: None; Roberto Nicosia: None; Kelly Smith: None

Background: Renal amyloidosis is an uncommon but problematic cause of proteinuria and nephrotic syndrome, which has very limited treatment options and usually leads to ESRD requiring renal replacement therapy. In this study, we assessed the incidence of different subtypes of amyloidosis over time in our patient population to better understand the etiology of renal amyloidosis.

Design: We reviewed our kidney biopsy database from 1984 through 2020 to define the incidence of renal amyloidosis and the subtypes of amyloid contributing to this disease. Amyloidosis subtype was correlated with clinical data.

Results: We observed a dramatic increase in serum amyloid A (AA) protein-type amyloidosis (Figure 1), beginning in 2000, and since 2015 AA is the most common renal amyloidosis subtype in our patient population. The increased incidence of AA-type amyloidosis was associated with heroin injection drug use (Figure 2); injection drug use-associated infections (skin and deep muscle abscesses, cellulitis, and osteomyelitis) were documented in over 85% of the cases. In a subset of patients (n=89) with extensive clinical data, renal biopsy was preceded by initial documentation of injection drug use associated infections (4.0 -18 years) and proteinuria (1.0 -14 years), and renal failure or death occurred 0.45 – 2.7 years after biopsy.

Figure 1 - 1080

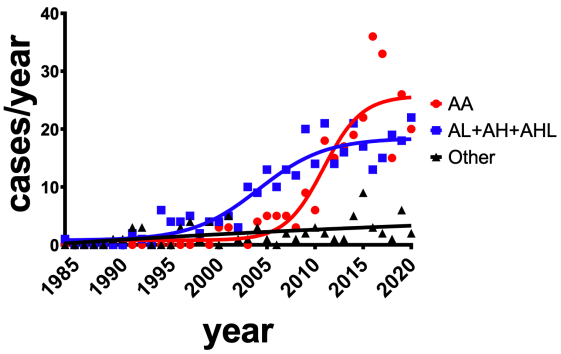

Figure 1. A surge in AA-type amyloidosis diagnosed in renal biopsies after 2000 in our institution. Shown are the number of cases diagnosed per year of AA-type (red), immunoglobulin-type (AL+AH+AHL) (blue) and other type (undetermined, ALECT2, APOA4, ALys) (black) amyloidosis. The lines represent four parameter logistic curve fits to the data (r-squared values: AA = 0.82, AL+AH+AHL = 0.89, Other = 0.22).

Figure 2 - 1080

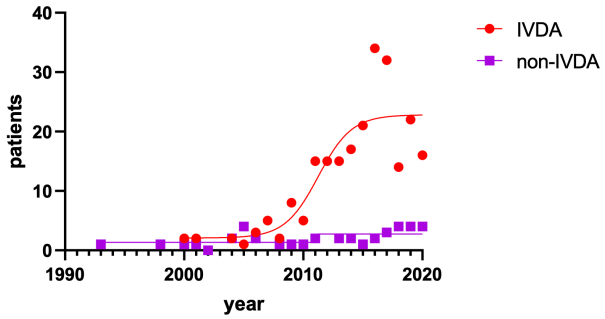

Figure 2. From the total number of cases diagnosed as AA amyloidosis (n=229) within the time period 1993-2020, there is a sharp increase in the number of cases related to skin infections secondary to heroin injection starting in the year 2000. The lines represent four parameter logistic curve fits to the data (r-squared values: IVDA = 0.79, non-IVDA = 0.56). IVDA: history of intravenous drug abuse.

Conclusions: Since 2000, there has been a dramatic increase in the incidence of AA-type amyloidosis, and in 2015 AA overtook AL amyloidosis as the predominant form of amyloidosis diagnosed in kidney biopsies at our institution. The dramatic increase in AA amyloidosis is associated with injection drug use and its infectious complications. Longitudinal data indicates repeated infections and asymptomatic proteinuria precede clinical presentation prompting biopsy by several years.

1081 EXT1 and NCAM1-associated Membranous Lupus Nephritis in a Cohort of Patients Undergoing Multiple Renal Biopsies

Paul Miller[1], Tiffany Caza[2], Chris Larsen[2], Vivek Charu[3]
[1]Stanford University Medical Center, Stanford, CA, [2]Arkana Laboratories, Little Rock, AR, [3]Stanford Medicine/Stanford University, Stanford, CA

Disclosures: Paul Miller: None; Tiffany Caza: None; Chris Larsen: None; Vivek Charu: None

Background: EXT1/2 and NCAM associated membranous lupus nephritis (MLN) may represent distinct disease phenotypes with prognostic significance.

Design: We searched our archives for patients with systemic lupus erythematous (SLE) and at least two renal biopsies demonstrating MLN. Each biopsy was stained for EXT1 and NCAM1 and scored as positive or negative for each. Biopsy and clinical data were reviewed.

Results: We identified 31 patients with a clinical diagnosis of SLE and at least two renal biopsies with MLN. 28 patients (90%) showed concordant staining for EXT1 and NCAM1 in both biopsies; 8 (26%) patients were EXT1-positive and NCAM1-negative, 18 (58%) patients were EXT1-negative and NCAM1-negative, and 2 (7%) patients were EXT1-negative and NCAM1-positive. Three patients (10%) had discordant EXT1 staining between their first and second biopsies (see figure 1); two patients (7%) were EXT1-positive in their first biopsy and EXT1-negative in their second biopsy and one patient (3%) was EXT1-negative in their first biopsy and EXT1-positive in their second biopsy. Comparing the EXT1-positive to EXT-negative cohort at the time of the first biopsy; the EXT1-positive cohort had a higher average eGFR (141 v. 111 ml/min/1.73m^2; p=0.04; see figure 2), lower average percent global glomerulosclerosis (0.5 v. 12%; p=0.05), lower average interstitial fibrosis and tubular atrophy (2.5 v. 11.7%; p=0.06), lower average total NIH chronicity scores (0.75 v. 2.33, p=0.05). On follow-up, the rate of change in eGFR did not significantly differ

between the two groups (p=0.24; see figure 2). One EXT1-positive patient (12.5%) developed CKDIV or ESKD compared to four patients (20%) in the EXT-negative group and two of the three EXT1-discordant patients (p=0.38).

		EXT-positive (n=8)		EXT-negative (n=18)		NCAM-positive (n=2)^		EXT-discordant (n=3)^	
		First biopsy	Last Biopsy	First biopsy	Last Biopsy	First biopsy	Last Biopsy	First biopsy	Last Biopsy
Age (median; IQR)		19.9 (13.6-35.3)	22.3 (14.5-42.5)	23.1 (16.3-34.7)	27.6 (19.5-37.8)	14.2, 42.0	16.2, 48.9	39.8, 25.0, 37.9	49.7, 36.0, 40.4
Interval between biopsies (years; median; IQR)			2.1 (1.5-5.9)		2.0 (1.5-4.0)		2.0, 6.8		9.9, 11.0, 2.5
Interval between first biopsy and last follow up (years; median; IQR)			11.9 (7.0-13.4)		6.7 (3.6-11.2)		6.3, 11.5		12.0, 15.3, 5.0
Sex	Female (n)	8		11		1		3	
	Male (n)	0		7		1		0	
Race/Ethnicity	Non-Hispanic Caucasian	1		0		1		0	
	Hispanic	1		8		0		1	
	African American	4		4		1		1	
	Asian/Pacific Islander	2		6		0		1	
Co-morbidities	Diabetes (Presumed type II)	1		1		0		0	
	Hypertension	1		6		1		1	
Serum Creatinine (median; IQR)		0.75 (0.6-0.8)	0.70 (0.6-0.8)	0.78 (0.58-0.90)	0.71 (0.60-1.4)	0.8, 2.1	0.7, 1.31	0.7, 0.7, 2.5	1.8. 5.0, 2.7
eGFR* (median; IQR)		140 (140-155)	145 (131-153)	127.1 (87.0-145.5)	118.8 (54.9-138.8)	128, 38	148, 64	118.2, 131.1, 36.6	42.7, 13.7, 32.9
eGFR* categories	>=90	5	8	11	9	1	1	2	0
CKD1	60-89	0	0	3	3	0	1	0	0
CKD2	45-59	0	0	0	0	0	0	0	0
CKD3	30-44	0	0	2	2	1	0	1	2
CKD4	15-29	0	0	1	1	0	0	0	0
CKD5	<15	0	0	0	1	0	0	0	1
	Missing	2	0	1	2	0	0	0	0
UPCR	>= 3 g/g	3	4	5	9	2	1	2	2
	< 3 g/g	2	4	9	6	0	1	0	0
	Missing	3	0	4	3	0	0	1	1
Hematuria	Yes	2	3	10	7	0	0	0	0
	No	1	2	3	6	0	0	0	0
	Missing	5	3	5	5	2	2	3	3
Biopsy characteristics	Class III	2	5	8	7	1	1	2	0
	Class IV	2	2	3	5	1	1	0	2
	NIH activity score (median; IQR)	3 (0-7)	3.5 (0.5-10.0)	2.5 (0.0-5.0)	1.5 (0-2.0)	6, 21	3,3	6,0,0	13,0,1
	NIH chronicity score (median; IQR)	0 (0-1.5)	2.5 (1.0-5.5)	2 (0-3)	3 (2-7)	1, 4	1,7	0,2,7	3,8,6
	%GS** (median; IQR)	0 (0-0)	6.1 (1.7-16.0)	2.9 (0-16)	7.9 (2.6-22.2)	0, 37.5		0,0,22	18.4, 46.9, 50.0
	%IFTA (median; IQR)	2.5 (0-5.0)	10 (2.5-35.0)	1 (0-10)	10 (5-30)	5, 15	1, 40	0,1,60	5,80,40

Figure 1 - 1081

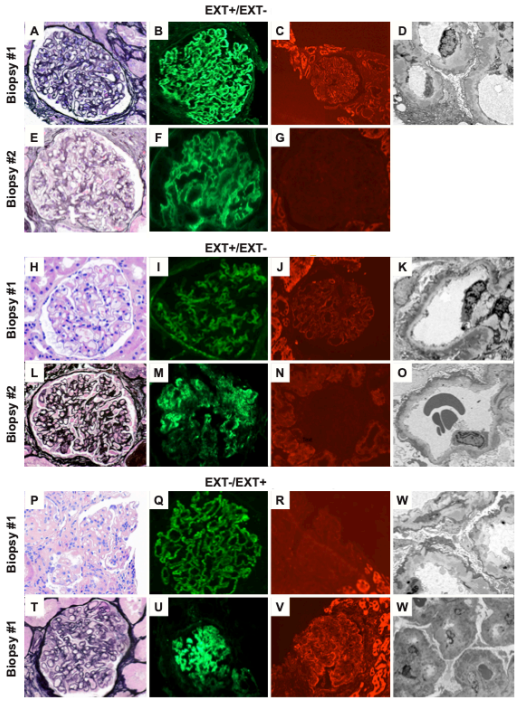

Figure 1: Representative histopathologic images of EXT-discordant cases. A, E, H, L, P, T Representative light microscopic images with basement membrane thickening and spikes and vacuoles seen on Jones silver stain (H&E & Jones silver; ×400); B, F, I, M, Q, U Representative IgG immunofluorescence with granular basement membrane staining (×400). C, J, V Representative EXT1 immunofluorescence with granular basement membrane staining (×400) G, N, R Representative negative EXT1 immunofluorescence staining (x 400). D, K, O, S, W Representative electron micrographs with electron-dense deposits along the subepithelial aspect of the glomerular basement membranes and podocyte foot process effacement.

Figure 2 - 1081

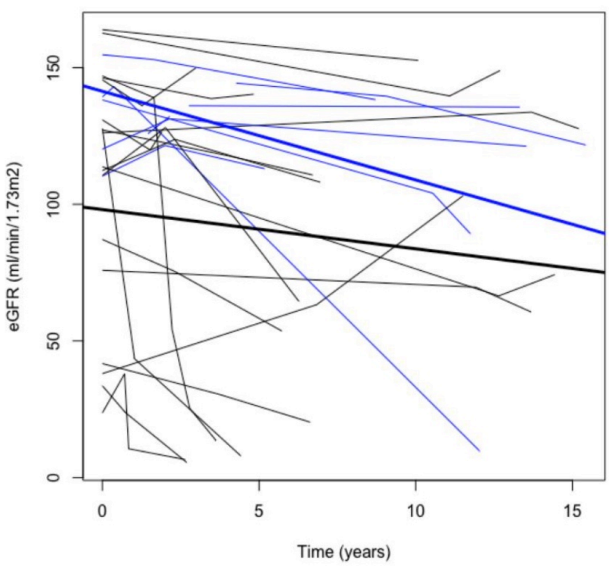

Figure 2: Longitudinal trajectories of eGFR over time in EXT-positive patients (blue), and EXT-negative patients (black). Bold lines represent model-based average trajectories for each group.

Conclusions: We performed the largest retrospective repeat-biopsy study to evaluate EXT1 and NCAM1 autoantigens in MLN. Our data confirm that EXT1-positivity is associated with better renal function at the time of diagnosis and raise the possibility that EXT1 status may change throughout the disease course of MLN.

1082 Amyloid Cast Tubulopathy, A Potential Rare Mimic of Light Chain Cast Nephropathy: A Report of 2 Cases from a Single Institution

Rusella Mirza[1], Xin Gu[2], Lisette Casagrande[3], Cara Rosenbaum[4], Rajib Kumar Gupta[5]
[1]Louisiana State University Shreveport, Shreveport, LA, [2]Louisiana State University Medical Center, Shreveport, LA, [3]Montclair, NJ, NJ, [4]New York-Presbyterian/Weill Cornell Medicine, New York, NY, [5]LSU Health Shreveport, Shreveport, LA

Disclosures: Rusella Mirza: None; Xin Gu: None; Lisette Casagrande: None; Cara Rosenbaum: None; Rajib Kumar Gupta: None

Background: Abnormal production of monoclonal light chains due to a lymphoproliferative neoplasm (plasma cell dyscrasia or B-cell lymphoma) can involve different compartments of the kidney in various ways, of which common subtypes include - light chain cast nephropathy (LCCN), AL-amyloidosis, monoclonal immunoglobin deposition disease, light chain proximal tubulopathy, etc. Amyloid cast tubulopathy (ACT) is an extremely rare subtype of monoclonal kidney disease in which AL-amyloid forms intra-tubular casts morphologically similar to LCCN. We report here 2 cases of ACT, both of which were associated with plasma cell dyscrasia.

Design: Patient #1 is a 49 year old male who presented with persistent abdominal discomfort and vomiting for couple of weeks. His workup revealed anemia, proteinuria, elevated creatinine, monoclonal gammopathy, lytic bone lesions and hypercalcemia, features consistent with multiple myeloma. Due to suspicion of myeloma-associated kidney damage, a kidney biopsy was performed. Patient #2 is a 54 year old male with a known history of inflammatory bowel disease and anemia, and found to have elevated creatinine, mild proteinuria and monoclonal gammopathy. A kidney biopsy was performed in suspicion of plasma cell dyscrasia-associated kidney damage. .

In both cases, biopsy cores were evaluated by light microscopy (LM), immunofluorescence (IF) and electron microscopy (EM). Congo red and Thioflavin-T were done to demonstrate presence of amyloid.

Results: Biopsies in cases 1 and 2 demonstrated normocellular glomeruli without evidence of glomerular paraprotein deposition. The principle pathological finding in both cases was sharp fractured intra-tubular casts staining for Congo red showing light chain restriction by IF and demonstrating a fibrillary composition on EM with average diameter consistent with that of amyloid, that is, between 7-12 nm (see figures 1 and 2).

Figure 1 - 1082

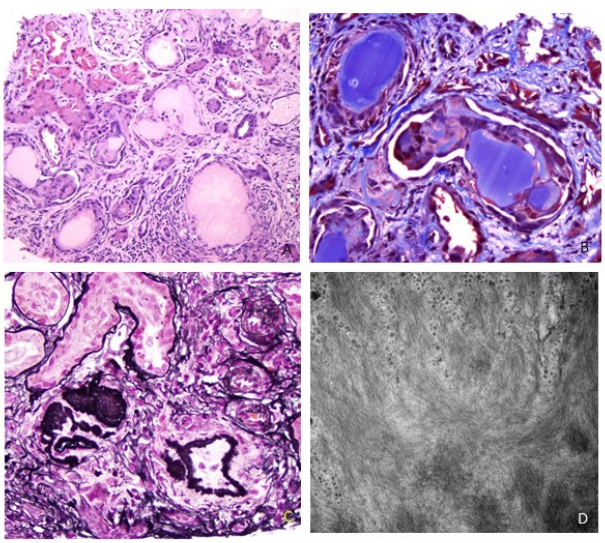

Figure 1 is biopsy of patient #1, tubules are distended by large casts that have elicited an impressive multinucleated giant cell and histiocytic reaction (A, B). The casts have a spicul periphery with silver stain (C), and amyloid fibrils by EM (D).

Figure 2 - 1082

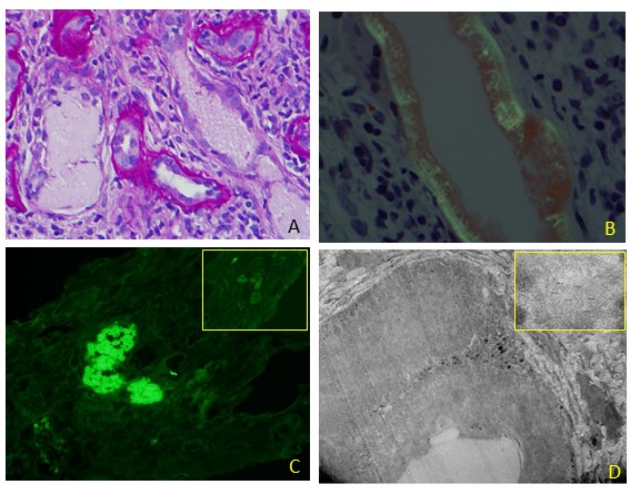

Figure 2 is biopsy of patient # 2, tubular casts are weak-PAS positive (A), Congo red positive with apple-green birefringence on polarized light (B), monoclonal positivity with lambda (C) with negative kappa (inset) and showing a large intra-tubular cast on EM which shows typical amyloid fibrils (D) on higher magnification (inset).

Conclusions: ACT is an extremely rare manifestation of a monoclonal kidney deposition disease superficially mimicking LCCN. In our institution with an average total kidney biopsy load of 3000 annually, we have diagnosed two such cases 11 years apart. Awareness of this entity is crucial to making the correct diagnosis and differentiating multiple myeloma with ACT (such as these two

cases), from the diagnosis of systemic AL amyloidosis with true parenchymal renal amyloid involvement as treatment differs between these entities.

1083 Proteinuria in Thrombotic Microangiopathy (TMA) Can Be Associated with Adaptive Partial Podocytopathy with Focal Podocyte Hyperplasia

Megan Moore[1], Olabisi Afolayan-Oloye[2], Wei Li[3], Hassan Kanaan[4], Ping Zhang[5]
[1]Oakland University William Beaumont School of Medicine, Rochester, MI, [2]Beaumont Health System, Royal Oak, MI, [3]William Beaumont Hospital, Royal Oak, MI, [4]Beaumont Health, Royal Oak, MI, [5]William Beaumont Hospital, Birmingham, MI

Disclosures: Megan Moore: None; Olabisi Afolayan-Oloye: None; Wei Li: None; Hassan Kanaan: None; Ping Zhang: None

Background: TMA associated renal failure is easy to understand, but it has been difficult to explain the significant proteinuria in some cases of TMA. We recently confirmed that 100% of hyperplastic podocytes in collapsing glomerulopathy stained positively for CD133 (a stem cell/progenitor marker) as previously reported. The goal of this study was to determine if there was significant fusion of foot processes (FFP) and CD133-positive hyperplastic podocytes in TMA to correlate with the proteinuria.

Design: The study included 12 negative controls (renal parenchyma away from renal cell carcinoma) and 25 TMA cases, either induced by drugs or due to other etiologies (preeclampsia, TTP, atypical HUS, malignant hypertension, etc). The percentage of FFP was estimated and proteinuria levels were obtained for TMA cases. Both groups of cases were stained for CD133 by immunohistochemical methods and the # of glomeruli with CD133-positive hyperplastic podocytes was analyzed.

Results: In total, 19 of 25 TMA cases had elevated protein/creatinine ratio more than 2 (Table). The TMA group had significantly higher levels of serum creatinine (2.81 ± 0.40 mg/dl) than the control group (0.95 ± 0.12 mg/dl). All controls showed positive CD133 staining only in the parietal epithelial cells (PEC), but none of them revealed positive CD133 staining in podocytes. In addition to positive CD133 staining in the PEC, 19 of 25 (76%) TMA cases showed positive CD133 staining in small clusters of hyperplastic podocytes within Bowman's space (Figure, orange arrows in B and D). The average percentage of glomeruli with CD133-positive hyperplastic podocytes was 12 % in the TMA group. This was significantly higher than in the control group (0 %) ($p = 0.0002$), although this positivity did not show significant correlation with proteinuria in TMA group ($r = 0.30$, $p = 0.1537$). The percent of FFP (56 ± 4 %) was significantly correlated with proteinuria (protein/creatinine ratio 4.4 ± 0.6) ($r = 0.46$, $p = 0.0237$) in the TMA group.

Table 1. CD133 Expression in Negative Controls And TMA Cases

	Brief history	Biopsy diagnosis	sCr (mg/dl)	Protein/Cr ratio	Fusion % by EM	CD133 intensity, +G/total G
Controls						
1	51M, biopsy for tumor	NSP	1.12	NA	NA	0
2	60M, biopsy for tumor	NSP	0.64	NA	NA	0
3	66F, biopsy for tumor	NSP	0.99	NA	NA	0
4	74F, biopsy for tumor	NSP	0.67	NA	NA	0
5	70M, nephrectomy for tumor	NSP	2.0	NA	NA	0
6	30F, nephrectomy for tumor	NSP	0.7	NA	NA	0
7	69M, nephrectomy for tumor	NSP	1.2	NA	NA	0
8	59F, nephrectomy for tumor	NSP	0.8	NA	NA	0
9	78F, nephrectomy for tumor	NSP	0.5	NA	NA	0
10	73 F, nephrectomy for tumor	NSP	0.8	NA	NA	0
11	84F, nephrectomy for tumor	NSP	1.2	NA	NA	0
12	61F, nephrectomy for tumor	NSP	0.8	NA	NA	0
Drug related						
1	54F, Infliximab (Crohn's disease)	TMA	1.97	1.6	20%	2+, 2/12
2	63M, Gemcitabine for cancer	TMA	3.23	4.28	60%	2+, 3/11
3	56M, intravitreal Bevacizumab	TMA	2.24	6.1	70%	0, 0/16
4	75F, systematic Bevacizumab	TMA	0.94	4.28	40%	3+, 9/31
5	78M, systematic Bevacizumab	TMA	2.48	2.4	70%	0, 0/14
6	82M, melanoma, with Opdivo	TMA	2.97	1.0	30%	3+, 2/11
7	47F, chemotherapy	TMA	3.54	0.61	30%	2+, 2/16

8	68M, chemotherapy	TMA	2.01	2.5	50%	0, 0/4
Other TMA						
9	30F with preeclampsia	TMA	5.59	8.95	80%	3, 3/15
10	50F with TTP	TMA	7.3	10.7	90%	3+, 2/14
11	58F with atypical HUS	TMA	7.56	0.15	50%	0, 0/6
12	81F, unknown	TMA	2.39	2	70%	2+, 1/10
13	73F, unknown	TMA	3.22	6.8	50%	3+, 2/13
14	35F with preeclampsia	TMA	1.93	4.2	40%	2+, 2/13
15	74F, thrombocytopenia	TMA	0.89	3.46	90%	0, 0/1
16	63M with hepatitis C	TMA	0.82	1.55	40%	3+, 1/23
17	28F with preeclampsia	TMA	3.23	4.36	70%	0, 0/6
18	78F with lupus thrombocytopenia	TMA	1.48	1.85	40%	2+, 2/29
19	41F preeclampsia	TMA	0.69	10	50%	3+, 2/17
20	27F, thrombocytosis	TMA	0.86	6.33	40%	2+, 1/5
21	53M, unknown	TMA	1.84	5.9	70%	2+, 2/14
22	68M, unknown	TMA	4.05	6.06	50%	3+, 1/19
23	65M, unknown	TMA	5.5	6.9	90%	2+, 3/18
24	81F, malignant hypertension	TMA	1.01	7.6	60%	3+, 1/13
25	46F, malignant hypertension	TMA	5.23	3.96	80%	2+, 1/3

NSP – no significant pathology, AIN – acute interstitial nephritis, TMA, thrombotic microangiopathy, PT – proximal tubules and G – glomeruli, NA – not available.

Figure 1 - 1083

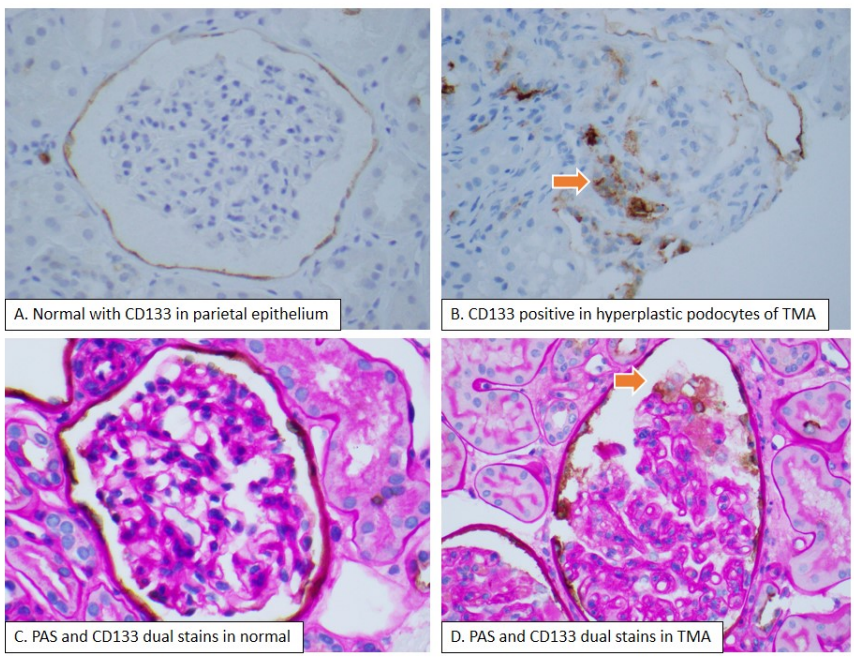

Conclusions: Our data indicate that the proteinuria in TMA can be associated with significant FFP. Small clusters of CD133-positive hyperplastic podocytes can be seen in the majority of TMA cases of this cohort, which supports an adaptive partial podocytopathy in some TMA cases.

1084 Peripheral Titer and Medulla Sampling Drive Biopsy Detection of Early BK Polyomavirus Nephropathy

Jahnavi Rajagopal[1], Madeline Vincent[1], Evan Farkash[1]
[1]University of Michigan, Ann Arbor, MI

Disclosures: Jahnavi Rajagopal: None; Madeline Vincent: None; Evan Farkash: *Consultant*, Novartis

Background: At our transplant center, BK polyomavirus treatment is protocol-driven, with the greatest immunosuppression reduction in patients with >100,000 copies/mL in serum or polyomavirus nephropathy (BKPVN) on biopsy. However, during the initial phase of polyomavirus nephropathy, the viral infection can be focal and potentially missed by random biopsy sampling. We hypothesized that detection of BKPVN on biopsy would be associated with deeper sampling (of medulla) and more advanced infection (higher peripheral BK PCR titers).

Design: 64 allograft biopsies during the initial phase of BK infection (initial positive or rising titers) were identified from kidney transplant recipients between 2010 and 2017. Biopsies were scored using the Banff 2017 classification. In addition, the extent of edema and plasma cell infiltrate, the number of cores containing cortex and medulla, and the absolute length of cortex and medulla were recorded. Histologic features were correlated with SV40 Large T Antigen staining and BK titer (Viracorp) at biopsy date. Statistical analyses were done by t-test in Excel.

Results: SV40-positive biopsies (BKPVN+, n=34) had a $\log_{10}$ BK titer of 4.30+/-0.99 copies/µL, versus 3.38+/-0.77 copies/µL for negative biopsies (BKPVN-, n=30) (p=0.00009). There was no difference in the number of cores with medulla (0.8+/-0.7 cores vs 0.8+/-0.9 cores, p=0.86) or the length of medulla (3.3+/-3.4 mm vs 3.7+/-4.7 mm, p=0.69) for BKPVN+ vs BKPVN- cases. 8 of the 34 BKPVN+ cases (23.5%) showed SV40 staining restricted to the medulla. BKPVN+ biopsies showed increased Banff i, ti, and t scores and more extensive plasma cell infiltrates (p=0.04, p=0.007, p=0.002, and p=0.0002).

Conclusions: Contemporaneous BK PCR titer, a rough proxy for the extent of the infection, is the most influential factor affecting the detection of polyomavirus nephropathy on biopsy. BK PCR $\log_{10}$ titers above 4.4 and below 3.39 were associated with very high and low pretest probabilities for sampling BKPVN. Although the amount of medulla present did not correlate with BKPVN detection, superficial sampling of only the cortex would have missed a quarter of the BKPVN cases. As expected, tubulointerstitial inflammation and plasma cell-rich inflammation was predictive of SV40 staining in the context of a positive BK PCR. We conclude that an indication biopsy adds the greatest diagnostic value in BKPVN management when BK PCR titers are intermediate, and that sampling of the medulla does add predictive value.

1085 Segmentation and Classification of Lymphocytes in the NEPTUNE Digital Kidney Biopsies via PatchSorter

Gina Sotolongo[1], Jihyeon Je[2], Xiang Li[2], Jarcy Zee[3], Bangchen Wang[4], Yijiang Chen[5], Tasneem Talawalla[5], Jeffrey Hodgin[6], Anant Madabhushi[5], Takaya Ozeki[6], Laura Mariani[7], Lawrence Holzman[8], Andrew Janowczyk[5], Laura Barisoni[2], Kyle Lafata[2]
[1]Duke University Health System, Durham, NC, [2]Duke University, Durham, NC, [3]The Children's Hospital of Philadelphia, Perelman School of Medicine at the University of Pennsylvania, Philadelphia, PA, [4]Duke University Medical Center, Durham, NC, [5]Case Western Reserve University, Cleveland, OH, [6]University of Michigan, Ann Arbor, MI, [7]Michigan Medicine, University of Michigan, Ann Arbor, MI, [8]Hospital of the University of Pennsylvania, Philadelphia, PA

Disclosures: Gina Sotolongo: None; Jihyeon Je: None; Xiang Li: None; Jarcy Zee: *Advisory Board Member*, Booz Allen Hamilton; Bangchen Wang: None; Yijiang Chen: None; Tasneem Talawalla: None; Jeffrey Hodgin: None; Anant Madabhushi: *Consultant*, Caris Inc, Roche, Cernostics; *Grant or Research Support*, AstraZeneca, Boehringer-Ingelheim, Bristol-Myers Squibb; *Stock Ownership*, Inspirata Inc, Elucid Bioimaging; Takaya Ozeki: None; Laura Mariani: *Consultant*, Travere Therapeutics, Calliditas Therapeutics, Reata; Lawrence Holzman: *Primary Investigator*, NIH; *Grant or Research Support*, NIH; Andrew Janowczyk: *Consultant*, Merck, Lunaphore, Roche; Laura Barisoni: *Consultant*, protalix; *Advisory Board Member*, vertex, Nephcure; Kyle Lafata: None

Background: In glomerular diseases, tubulointerstitial changes such as interstitial fibrosis, inflammation, and tubular injury, have prognostic and predictive value. The renal biopsy evaluation and reporting for interstitial inflammation is based on visual assessment using a semiquantitative scale. However, this approach does not provide a quantitative measure of the topology or number of inflammatory cells present and is often poorly reproducible. This study aims to develop a pipeline (Fig 1) for the automatic detection and characterization of lymphocytic inflammation on whole slide images (WSIs) of kidney biopsies.

Design: 15 H&E WSIs from the NEPTUNE digital pathology repository were used. From each WSI, two 1024x1024 pixel tiles were visually identified as regions of high lymphocytic inflammation. A pretrained deep learning (DL) detection algorithm based on the *StarDist* architecture was applied to each tile to identify all nuclei. Each tile was then processed into a set of 32x32 pixel patches, each containing a single nucleus. Using the open-source software, *PatchSorter*, each patch was manually labelled as either a lymphocyte or non-lymphocyte by a pathology resident. Each label was then reviewed by a senior renal pathologist. The matched {H&E, label} patches were used as DL training samples (i.e., paired data examples of model input and desired model output). These patches were then divided into training (80%) and validation (20%) cohorts based on a stratified Monte Carlo sub-sampling technique and used to train and tune a ResNet50 DL classifier, respectively. Data augmentation was applied to increase the diversity of the training data. Training consisted of 200 epochs and the model with the lowest validation loss was independently tested on different patches from a separate WSI. Diagnostic test characteristics were calculated to quantify model performance.

Results: A total of 9362 nuclei (2048 lymphs and 7314 non-lymphs) across 14 WSIs were annotated on the training dataset. The testing dataset included 203 lymphocytes and 1108 non-lymphocytes from 1 WSI. An example of the model applied to the test image is shown in Fig 2. The accuracy of the model was 78%, the recall (sensitivity) was 83%, the precision (positive predictive value) was 39%, and the area under the ROC curve (AUC) was 87% (Fig 2).

Figure 1 - 1085

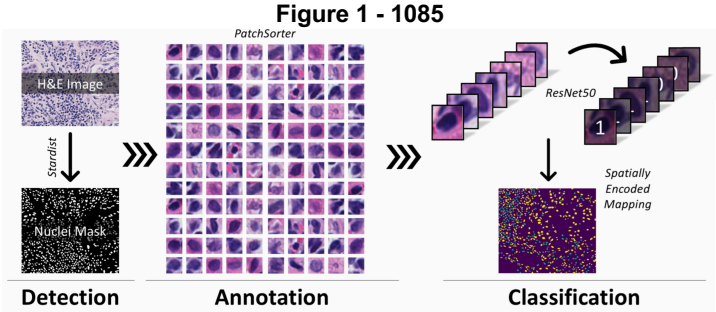

Figure 1. Deep learning (DL) framework to detect and classify lymphocytic inflammation on digitized renal biopsies. The pipeline includes: **(1)** a nuclei detection step that automatically identifies all nuclei on an input H&E based on the *Stardist* DL architecture; **(2)** an annotation step to label lymphocytes via *PatchSorter* and curate a DL training dataset; and **(3)** a lymphocyte classification model training step based on the ResNet50 DL architecture.

Figure 2 - 1085

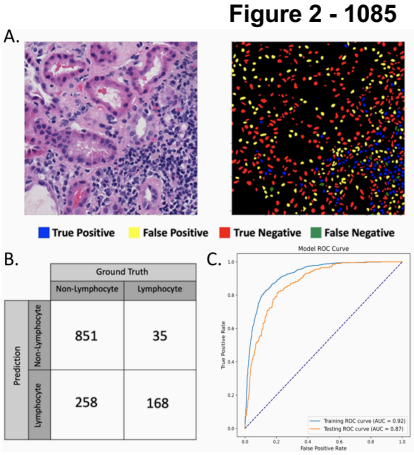

Figure 2. Nuclei classification modeling results applied to testing dataset.

(A) Color-coded model performance results (testing data), relative to corresponding input H&E image.

(B, C) Model performance statistics results, including **(B)** testing data confusion matrix and **(C)** ROC curve for both training and testing datasets.

Conclusions: These preliminary data demonstrate that DL can be used as a tool to automatically assist pathologists in identifying and quantifying lymphocytic inflammation on renal H&E WSIs.

1086 Novel Diagnostic Methodologies in Non-Polyoma Infections in Renal Allograft Biopsies

Ramya Krishna Velagapudi[1], Meghan Kapp[1], Anthony Langone[1], Harold Helderman[1], Paisit Paueksakon[1], Mark Lusco[1], Agnes Fogo[1]
[1]*Vanderbilt University Medical Center, Nashville, TN*

Disclosures: Ramya Krishna Velagapudi: None; Meghan Kapp: None; Anthony Langone: None; Harold Helderman: None; Paisit Paueksakon: None; Mark Lusco: None; Agnes Fogo: None

Background: Transplant patients are prone to unusual infections and may have biopsies to rule out infection and/or rejection. Identification of the organism may require broad and novel diagnostic testing. We evaluated the spectrum of infectious organisms and techniques required for their identification in renal allograft biopsies.

Design: Allograft renal biopsies in our laboratory from January 2015 to August 2021 with findings suspicious for infection including acute pyelonephritis or necrotizing granulomatous inflammation were identified. Polyoma virus nephropathy (PVN) cases were excluded. The clinical history, histologic findings, diagnosis, and ancillary testing on blood, urine and/or biopsy tissue were reviewed.

Results: 99 biopsies (3.1%) from 93 patients met criteria from 3207 reviewed. 10 (10.1%) biopsies showed necrotizing granulomatous inflammation and 89 (89.9%) showed acute pyelonephritis. An organism was identified in 4 of 10 cases with

necrotizing granulomas and in 20 of 89 cases with acute pyelonephritis. 10 had unusual etiologies (Table 1). Additional testing required for organism diagnosis varied based on infectious etiology and included immunohistochemistry (IHC), electron microscopy (EM), polymerase chain reaction (PCR) on blood, urine, and tissue for adenovirus, GMS for fungi, tissue PCR for Mycobacterium, and a broad PCR panel for fungal organisms on tissue that identified Zygomycete from Cunninghamella family. One patient with granulomatous interstitial inflammation and no infectious etiology identified despite extensive testing on blood, urine and tissue, by IHC, cultures, PCR and serology, benefitted from glucocorticoids and clinically improved. In 3 biopsies, the patient's urine grew less than 100,000 CFU of Enterococci, E. coli or Klebsiella at >5days, yet the biopsy confirmed acute pyelonephritis leading to specific treatment and clinical improvement.

Table 1: Etiology based on morphologic findings and specific ancillary testing methods used

Morphologic findings	Etiology	Ancillary testing
Necrotizing granulomatous inflammation (10/99)	Adenovirus (2/10 = 20%)	Adenovirus IHC, EM for viral particles
	Histoplasma (1/10 = 10%)	GMS stain on allograft biopsy
	Mycobacterium tuberculosis (TB) (1/10 = 10%)	Minimal adenovirus by IHC stain and no viral particles by EM, despite positive PCR on blood and urine. Negative PCR for TB, but response to TB treatment based on history of TB pre transplant
	6 biopsies (6/10 = 60%)	Diagnostic testing without identifiable infectious etiology
Acute pyelonephritis (89/99)	Escherichia coli UTI (7/89 =7.9%)	Urine cultures (10,000-25,000 CFU in 1)
	Bacteremia (Staphylococci, Enterococci, Escherichia coli) (3/89 = 3.4%)	Urine and blood cultures
	Enterococcal UTI (2/89 = 2.2%)	Urine cultures (10,000-49,000 CFU)
	Candida UTI (2/89 = 2.2%)	Urine cultures
	CMV nephropathy (1/89 = 1.1%)	CMV IHC
	Zygomyces (Cunninghamella family) (1/89 = 1.1%)	Broad panel PCR on renal biopsy tissue
	Klebsiella UTI (1/89 = 1.1%)	Urine cultures (10,000-25,000 CFU)
	Proteus UTI (1/89 = 1.1%)	Urine cultures
	Pseudomonas UTI (1/89 = 1.1%)	Urine cultures
	Clostridium difficile (1/89 = 1.1%)	Stool C. difficile toxin gene detection
	69 biopsies (69/89 = 77.5%)	Unknown etiology at the time of biopsy (17 presumed bacterial infection clinically)

Conclusions: Non-PVN infectious etiologies are relatively rare in allograft biopsies as most patients are diagnosed by clinical symptomatology, urine and blood cultures. 10% of biopsies required extensive additional testing and modification of existing diagnostic criteria to reveal the rare source of the infection. Clinical-pathologic correlation and use of novel tests as indicated can unveil unusual etiologies so treatment can be directed accordingly.

1087 Renal Biopsy Findings in Syphilis: A 10-Year Institutional Experience

Simon Walker[1], Jean Hou[2]
[1]Calgary, Canada, [2]Cedars-Sinai Medical Center, Los Angeles, CA

Disclosures: Simon Walker: None; Jean Hou: None

Background: Syphilis is a re-emerging health issue in both the United States and Canada, with systemic health manifestations including renal disease. There are rare and small case series describing the renal pathologic findings, which are quite varied. With the increasing incidence of syphilis infections, further characterization of syphilis-related pathologic features is needed to educate renal pathologists about the heterogeneity of renal biopsy findings.

Design: We searched our institution's database for renal biopsies in patients with a reported clinical history of syphilis. A clinical history from the referring clinician stating active, latent or previous clinical history was required for inclusion. Patients with rapid plasma regain (RPR) positivity and no other findings of syphilis were excluded. Demographic information and diagnostic report data were abstracted and the dominant histologic abnormality of each case was assessed. Ancillary studies are pending at the time of abstract submission.

Results: We identified 30 biopsies from 29 patients. The majority of cases (90%) occurred in the last 5 years, consistent with current epidemiologic trends. Our cohort was 73 percent male and the mean age was 44 years old. 37% of cases were reported as

HIV positive and 57% cases did not report the HIV status. Histologic findings ranged from mild to significant disease, with one biopsy showing no pathologic changes. The primary diagnoses varied, with 8 (27%) biopsies showed focal and segmental glomerulosclerosis (including collapsing FSGS), 4 biopsies (13%) showed a membranous pattern and 4 (13%) biopsies showed immune complex glomerulonephritis.

Conclusions: We report the largest case series to date of renal biopsies in individuals diagnosed with syphilis. The histologic presentation of syphilis is varied and can be challenging for renal pathologists. A high index of clinical suspicion and good communication with clinicians is essential for correct diagnosis.

1088 Post COVID-19 Histopathologic Findings in Renal Transplants

Shuling Zheng, Case Western Reserve University/University Hospitals Cleveland Medical Center, Cleveland, OH

Disclosures: Shuling Zheng: None

Background: Background: Renal dysfunction has been reported in patients infected with the novel coronavirus, SARS-CoV-2, which causes coronavirus disease 2019 (COVID-19). A spectrum of histopathologic changes has been identified in the kidneys, especially native kidneys. However, there are limited data for transplant kidneys. Multiple studies have shown no evidence of direct viral infection of renal cells by immunohistochemistry, in situ hybridization and ultrastructural examination. The association of morphologic changes with this infection and the underlying mechanism remain undefined currently. This study is aimed to report important pathologic findings in renal transplants after recipients were diagnosis with COVID-19.

Design: Design: Medical records and pathology data were retrieved and retrospectively analyzed from renal transplant patients diagnosed with COVID-19 during 11/2020-5/2021 in our institution. All renal biopsies were processed for light, immunofluorescence and electron microscopy according to a standard protocol.

Results: Results: Six for-cause renal transplant biopsies were identified post COVID-19 and 2-29 months post transplant in four patients, including a 12 year-old (yo) multiracial male (M), a 25 yo white M, a 62 yo white female with the second transplant kidney and a 33 yo white M. All patients survived COVID-19 without intubation. Patient 1's biopsy 13 days post COVID-19 showed de novo immune complex deposition, 1B acute T-cell mediated rejection (TCMR) and focal segmental glomerulosclerosis (FSGS) and the biopsy 65 days post COVID-19 revealed much weaker immune complex deposition and much less tubulointerstitial inflammation. Patient 2's biopsy 55 days post COVID-19 demonstrated de novo immune complex deposition and no acute rejection. Patient 3's biopsy 49 days post COVID-19 showed acute tubular injury (ATI) and the biopsy 134 days post COVID-19 revealed FSGS. Patient 4 had 1B chronic active TCMR, chronic active antibody mediated rejection (ABMR), ATI and FSGS 182 days post COVID-19. No collapsing glomerulopathy or endothelialitis was identified in these biopsies.

Conclusions: Six renal transplant biopsies 13-182 days post COVID-19 in 4 recipients revealed de novo immune complex deposition (2/4), de novo DSAs (1/4), ATI (2/4), 1B acute TCMR (1/4), 1B chronic active TCMR and chronic active ABMR (1/4) and FSGS (2/4). More data are needed to further investigate the potential association of histopathologic findings in renal transplants with COVID-19.